



Advancing Estimation of Hepatobiliary Clearances in Physiologically Based Pharmacokinetic Models of Rosuvastatin Using Human Hepatic Concentrations

Li Wang¹ · Zhiyao Zhu¹ · Doanh Tran¹ · Shirley K. Seo¹ · Xiaolei Pan¹

Received: 20 September 2021 / Accepted: 6 November 2021 / Published online: 3 December 2021

This is a U.S. government work and not under copyright protection in the U.S.; foreign copyright protection may apply 2021

ABSTRACT

Purpose To estimate hepatobiliary clearances of rosuvastatin via simultaneously fitting to reported human positron emission tomography (PET) data in the liver and gallbladder.

Methods A hepatobiliary model incorporating five intrinsic hepatobiliary clearances (active uptake clearance at the sinusoidal membrane, efflux clearance by passive diffusion through the sinusoidal membrane, influx clearance by passive diffusion through sinusoidal membrane, clearance of biliary excretion at the canalicular membrane, and intercompartment clearance from the intrahepatic bile duct to the gallbladder) and three compartments (liver, intrahepatic bile duct, and gallbladder) was developed to simultaneously fit rosuvastatin liver and gallbladder data from a representative subject reported by Billington et al. (1). Two liver blood supply input functions, arterial input function and dual input function (using peripheral venous as an alternative to portal vein), were assessed. Additionally, the predictive performance between the established model and

four reported models trained with only systemic exposure data, was evaluated by comparing simulated liver and gallbladder profiles with observations.

Results The established hepatobiliary model well captured the kinetic profiles of rosuvastatin in the liver and gallbladder during the PET scans. Application of dual input function led to a marked underestimation of liver concentrations at the initial stage after *i.v.* dosing which cannot be offset by altering model parameter values. The simulated hepatobiliary profiles from three of the reported models demonstrated substantial deviation from the observed data.

Conclusions The present study highlights the necessity of using hepatobiliary data to verify and improve the predictive performance of hepatic disposition of rosuvastatin.

KEY WORDS Hepatobiliary clearance · membrane transporters · PET imaging · PBPK modeling · [¹¹C] rosuvastatin

ABBREVIATIONS

AIC	Akaike's Information Criterion
AIF	arterial input function
BCRP	breast cancer resistance protein
CsA	cyclosporin A
CL _{bile}	clearance of biliary excretion at the canalicular membrane
CL _{gall}	intercompartment clearance from the intrahepatic bile duct to the gallbladder
DDI	drug interaction
DIF	dual input function
IVIVE	<i>in vitro</i> to <i>in vivo</i> extrapolation
MATE	multidrug and toxic compound extrusion

Supplementary Information The online version contains supplementary material available at <https://doi.org/10.1007/s11095-021-03138-1>.

✉ Xiaolei Pan
Xiaolei.Pan@fda.hhs.gov

¹ Division of Cardiometabolic and Endocrine Pharmacology, Office of Clinical Pharmacology, Office of Translational Sciences, Food and Drug Administration, 10903 New Hampshire Ave, Silver Spring, MD 20993, USA

NTCP	sodium/taurocholate cotransporting polypeptide
OATP	organic anion transporting polypeptide
OCT	organic cation transporter
P-gp	P-glycoprotein
Q_H	hepatic blood flow
V_{GAL}	gallbladder volume
V_{IBD}	intrahepatic bile duct volume
V_{HC}	volume of hepatocytes
V_{HE}	volume of hepatic extracellular space

INTRODUCTION

Intracellular drug concentrations are fundamentally important to the understanding of drug efficacy, toxicity, and drug interactions (DDIs) (2). As it is impractical to quantify intracellular drug concentrations in routine clinical pharmacokinetic studies, systemic exposure (blood or plasma drug concentrations) has been commonly used as a surrogate measure, assuming that unbound drug concentrations in the systemic circulation are equal to unbound intracellular drug concentrations at the site of action. However, such an assumption might not be valid when transporter-mediated disposition is involved. Transporters that mediate the flux of drugs, metabolites, and endogenous compounds across cellular membranes can result in intracellular levels of unbound substrate drugs substantially different from the levels in the extracellular environment (2). This disconnect makes it difficult to accurately predict drug response for drugs whose primary pharmacological action is dependent on unbound drug molecules interacting with intracellular targets. For example, the glucose-lowering effect of metformin is altered when organic cation transporter (OCT)/ multidrug and toxic compound extrusion (MATE)-mediated hepatic transport is inhibited, while minimal or no alterations in metformin systemic exposure is observed (3, 4).

To address this issue, physiologically-based pharmacokinetic (PBPK) modeling has been increasingly used to predict both systemic and tissue concentrations (2, 5). Transport clearances are incorporated into tissue submodels (e.g., liver and kidney) to reflect the impact of transport processes on drug distribution and elimination. Though intrinsic transport clearances can be obtained from *in vitro* assays, simply applying the *in vitro* to *in vivo* extrapolation (IVIVE) framework for scaling *in vitro* transporter kinetic data to *in vivo* is not sufficient to accurately capture plasma concentration-time profiles in most cases, and empirical scaling factors are needed (6, 7). Therefore, estimation of transport clearances for PBPK modeling relies on clinical

pharmacokinetic data. This “middle-out” approach, however, raises the issue of whether systemic exposure profiles are sufficient to support estimation of clearance of transporters, given that some transporter clearances might not be sensitive to the change in systemic concentration. Simulations have shown that when canalicular efflux and/or metabolic clearance is much greater than sinusoidal efflux clearance, the systemic exposure is merely determined by sinusoidal uptake (8). In other words, sinusoidal uptake clearance is the only hepatobiliary clearance which can be accurately estimated when the PBPK model is trained with systemic pharmacokinetic data. In addition, there have been a variety of liver submodels reported to describe hepatic distribution and disposition (6, 9–11). Although these models were verified based on the blood/plasma data, the performance in predicting liver pharmacokinetics has not been confirmed. Collectively, it is necessary for further verification/refinement of liver submodels to evaluate and improve their predictive performance when liver pharmacokinetic profiles become available.

Over the last two decades, there has been increasing information on quantitative tissue data obtained from noninvasive nuclear imaging methods for several transporter probe drugs, including rosuvastatin (RSV) (1, 2). Multiple transporters are involved in the hepatic uptake and biliary excretion of RSV. Specifically, organic anion transporting polypeptides (OATPs) and sodium/taurocholate cotransporting polypeptide (NTCP) are the major contributors to sinusoidal active uptake (12, 13), while breast cancer resistance protein (BCRP), P-glycoprotein (P-gp), and multidrug resistance-associated protein (MRP)2 dominate the biliary efflux of RSV (14). Because of its safety profiles, unique disposition properties, and well characterized pharmacokinetic profiles in various patient populations, RSV is frequently used as an *in vivo* probe substrate to determine the DDI potential for new molecular entities that are OATPs or BCRP inhibitors. It is critical to verify these PBPK models of RSV with tissue exposure data to increase the confidence in the model prediction.

In the present study, hepatobiliary clearances of RSV were estimated via simultaneously fitting to previously published human [^{11}C]RSV liver and gallbladder concentration profiles measured by positron emission tomography (PET) imaging, under both control and DDI conditions (1). As portal venous concentration cannot be determined, two liver input functions, using either arterial concentrations or arterial/peripheral venous concentrations (1:4 according to the contribution of hepatic artery and portal vein to total liver blood supply) were tested as the model input. In addition, four reported liver submodels of RSV were selected

to simulate hepatobiliary profiles. The model performance in predicting liver pharmacokinetics was examined by comparing the simulation with the observed hepatic disposition data.

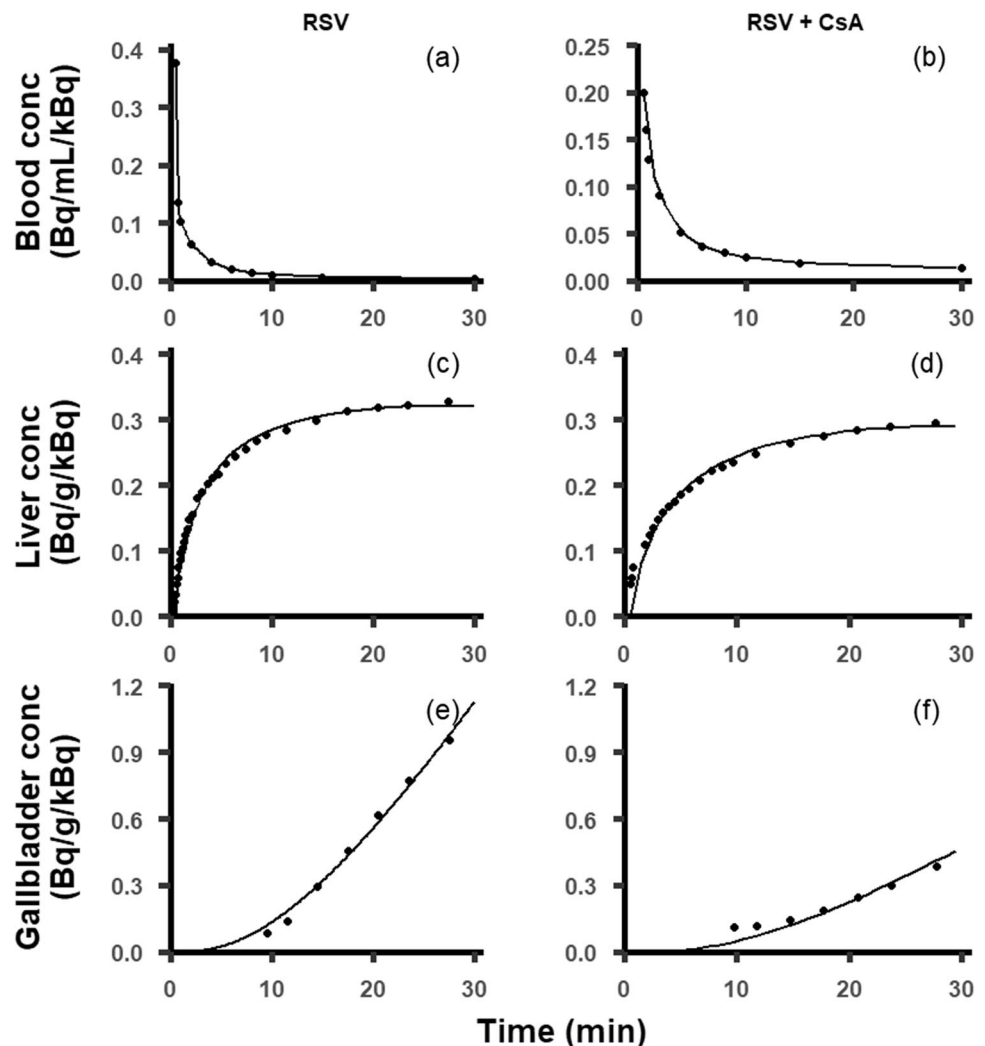
MATERIALS AND METHODS

Description of Datasets

Clinical datasets describing hepatobiliary disposition of [^{11}C]RSV were previously published by Billington *et al* (1). In brief, six healthy subjects without carrying polymorphic SLCO1B1/ABCG2 genotypes (i.e., SLCO1B1 c.521TC, c.521CC, c.1463CC; ABCG2 c.421AA) were enrolled in the study. All subjects received three doses of RSV during the study, including an initial oral dose of 5 mg, followed by two *i.v.* injections of [^{11}C]RSV with 2-h interval after ~ 2.5 h. The dosing regimen was designed to ensure that pharmacokinetics of [^{11}C]RSV

were reflective of that at a clinically relevant dose level. Morphine (0.04 mg/kg, *i.v.*) was given immediately prior to each *i.v.* dose of [^{11}C]RSV to prevent emptying of the gallbladder during imaging. Plasma concentrations of [^{11}C]RSV lactone and [^{11}C]polar metabolites during the imaging period were measured. The hepatobiliary disposition of [^{11}C]RSV was determined in the absence (the control condition) and presence (the DDI condition) of cyclosporin A (CsA), which is known as an inhibitor of OATPs, NTCP, MRP2, BCRP, and P-gp (1). CsA was administered as an *i.v.* infusion (2.5 mg/kg/h) about 45 min prior to the second *i.v.* dose of [^{11}C]RSV. Though the complete pharmacokinetic profiles including dose-normalized radioactivity concentration vs. time curves in the arterial/venous blood, liver, and gallbladder were available from single subject (Figs. 1 and 2), the hepatobiliary disposition of [^{11}C]RSV in the selected subject was representative of that in participant population via comparing hepatic and gallbladder [^{11}C]RSV concentration vs. time curves among these

Fig. 1 Dose-normalized radioactivity concentration vs. time profiles in the arterial blood (a and b), liver (c and d), and gallbladder (e and f) in a representative subject under both control and DDI (with CsA) conditions reported by Billington *et al.* (1). Solid lines in (c–f) represent the model fit to the liver and gallbladder concentrations



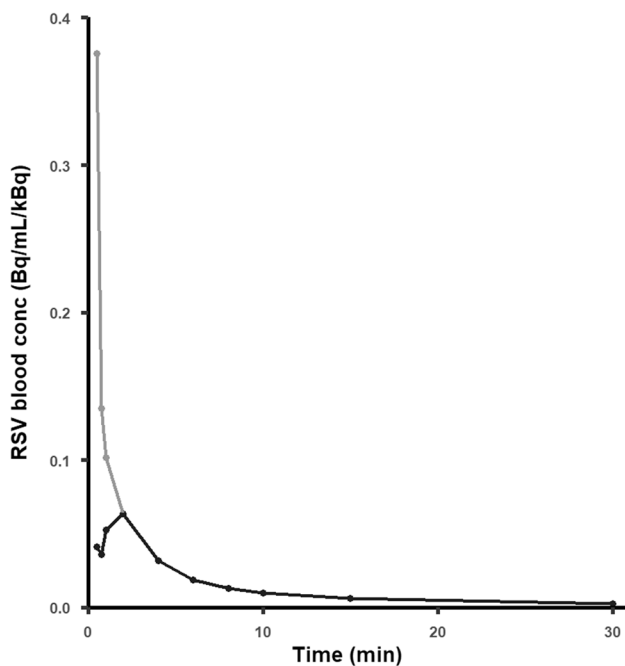


Fig. 2 Dose-normalized radioactivity concentration vs. time profiles in the arterial (gray circle) and venous (solid circle) blood samples under control condition. The concentrations in arterial and venous blood differed until 4 min after *i.v.* administration of RSV

participants (Fig. 3). All concentration-time data were digitized using DigitizeIt version 2.5.3.

Pharmacokinetic Modeling

The basic structure of the liver model of RSV has been previously reported (6, 10, 11). Briefly, the liver model was divided into 5 sequential pairs of 2 sub-compartments (extrahepatic and hepatocellular compartments) that were connected by hepatic blood flow in tandem, which mimic the hepatic disposition process according to the dispersion model. To describe the biliary excretion process during the imaging period, two compartments that represented the intrahepatic bile duct and gallbladder were added to the liver model. The radioactivity measured in the regions of interest of the liver was assumed to be the sum of the radioactivity present in the liver compartment (5 sequential pairs) and the intrahepatic bile duct compartment. Five intrinsic hepatobiliary clearances, including active uptake clearance at the sinusoidal membrane (PS_{act}), efflux clearance by passive diffusion through the sinusoidal membrane ($PS_{dif,eff}$), influx clearance by passive diffusion through sinusoidal membrane ($PS_{dif,inf}$), clearance of biliary excretion at the canalicular membrane (CL_{bile}), and intercompartment clearance from the intrahepatic bile duct to the gallbladder (CL_{gall}) were incorporated in the model to describe the transfer of unbound RSV from

the blood to the gallbladder. The hepatic metabolism of RSV was not considered as plasma concentrations of RSV metabolites during the imaging period were negligible (1). Additionally, transporter-mediated efflux at the sinusoidal membrane was not incorporated in the model due to the limited evidence of its importance in humans (10, 15). The ratio of $PS_{dif,inf}$ over $PS_{dif,eff}$ was set as 0.25 as suggested by a previous report (10). The model parameters, including hepatic blood flow (Q_H), intrahepatic bile duct volume (V_{IBD}), gallbladder volume (V_{GAL}), volume of hepatocytes (V_{HC}), volume of hepatic extracellular space (V_{HE}) are shown in Table I. The details of the liver model, including model structures, equations, and assumptions are described in the Supplemental Materials.

The blood supply of the liver was used as the forcing function in the liver model of RSV. The liver receives a blood supply from both the hepatic artery and the portal vein. However, the portal vein cannot be sampled in humans. Two approaches were tested in this study including arterial input function (AIF) and dual input function (DIF). Arterial input was used as a surrogate in AIF, while DIF took the contribution of the portal vein to the liver blood supply into account (the portal vein and hepatic artery contribute 80% and 20% of the total liver blood supply) and utilized peripheral venous as an alternative to portal vein (16). The hepatic input blood concentrations of [^{11}C]RSV (C_B) were estimated using Eq. 1, assuming that the radioactivity concentrations in peripheral venous blood could mimic that in portal vein. $C_{Arterial}$ and C_{Venous} represent the [^{11}C]RSV concentrations in arterial and peripheral venous blood samples, respectively.

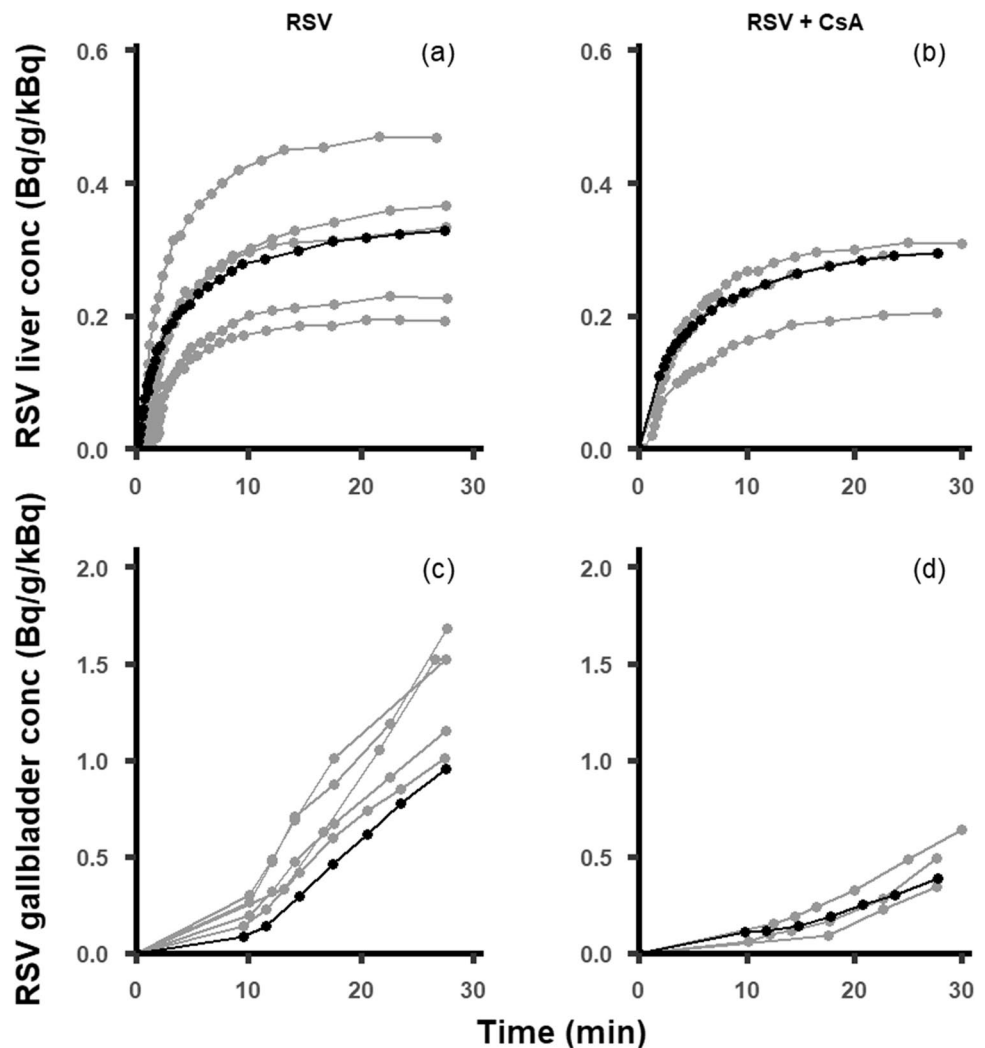
$$C_B = C_{Venous} \times 0.8 + C_{arterial} \times 0.2 \quad (1)$$

The values of human physiological parameters (e.g., volume of intrahepatic bile duct (V_{IBD}), gallbladder (V_{GAL}), hepatocytes (V_{HC}), and hepatic extracellular space (V_{HE}), as well as hepatic blood flow (Q_H) and drug-specific parameters (e.g., unbound fraction in the blood (f_B) and liver (f_H)) were consistent with previously reported (17–20). Hepatobiliary clearances including PS_{act} , $PS_{dif,eff}$, and CL_{bile} reported by Jones *et al.* was used as initial estimates. (6) CL_{gall} was assumed to be equal to CL_{bile} at initial modeling.

Simulation of the Hepatobiliary Disposition Profiles of RSV with Reported Liver Models

Four liver submodels from reported PBPK models of RSV were selected for the purpose of predictive performance comparison (6, 9–11). The selected

Fig. 3 Dose-normalized radioactivity concentration vs. time profiles in the liver (a and b) and gallbladder (c and d) in all subjects under both control and DDI (with CsA) conditions reported by *Billington et al.* (1). The black circles represent the concentration profiles used for modeling in the present study, while the gray circles represent the concentration profiles in the remaining subjects



liver models equipped the similar model structure (sequential pairs of two sub-compartments that were connected by hepatic blood flow in tandem) with minor modifications: The liver model reported by *Li et al.* assumed a permeability-limited distribution between intracellular liver sub-compartments; The liver model developed by *Bosgra et al.* applied four sequential pairs of two sub-compartments while other model applied five sequential pairs; The ratio of $PS_{\text{dif,inf}}$ over $PS_{\text{dif,eff}}$ was set as 0.25 in the liver model published by *Futatsugi et al.*, while the two parameters were assumed equal in other liver models (6, 9–11). In addition to the model structures, the selected studies applied different methods for estimation of hepatobiliary clearances of RSV: Scaling *in vitro* hepatobiliary clearance and fitting of *i.v.* clinical data to establish empirical scaling factors (*Jones et al.*); A global optimization approach to obtained empirical scaling factors based on *i.v.* clinical data (*Li et al.*); Scaling *in*

vitro hepatobiliary clearance and simultaneous fitting of clinical data for *p.o* and *i.v.* administered RSV to obtain scaling factors (*Futatsugi et al.*); Scaling *in vitro* PS_{act} (based on the transporter protein expression levels) and $PS_{\text{dif,eff}}$, while estimating CL_{bile} via fitting to clinical *p.o* and *i.v.* data (*Bosgra et al.*) (6, 9–11). The reported parameter values in these studies were fixed for the simulation (shown in Table S1 in the Supplemental Materials). In order to simulate hepatobiliary disposition data by PET imaging, the intrahepatic bile duct compartment and gallbladder compartment were added to these liver models. The details of the selected liver submodel and model parameters are described in the Supplemental Text. The predictive performance among the selected models was evaluated by comparing simulated hepatic and gallbladder profiles with observations.

Table 1 Physiological Parameters and Initial Estimates of Rosuvastatin Hepatobiliary Clearances

Parameter	Value	Reference/comments
Physiological parameters		
Q_H (L/h/kg)	1.24	(19)
V_{IBD} (mL/L liver)	3.2	(18)
V_{GAL} (L/kg)	0.000257	(27)
V_{HC} (L/kg)	0.0174	(19, 20)
V_{HE} (L/kg)	0.00669	(19, 20)
Fixed parameters for RSV		
f_B	0.174	(10)
f_H	0.179	(10)
Initial parameters for RSV		
PS_{act} (L/h)	1.190	(6)
$PS_{dif,eff}$ (L/h)	1.7	(6)
$PS_{dif,inf}$ (L/h)	0.43	Assuming the ratio of $PS_{dif,inf}$ over $PS_{dif,eff}$ was 0.25
CL_{bile} (L/h)	1.2	(6)
CL_{gall} (L/h)	1.2	Assuming CL_{gall} is equal to CL_{bile}

Abbreviations: Q_H : Hepatic blood flow; V_{IBD} : Intrahepatic bile duct volume; V_{GAL} : Gallbladder volume; V_{HC} : Volume of hepatocytes; V_{HE} : Volume of hepatic extracellular space; f_B : Protein unbound fraction in blood; f_H : Hepatic protein unbound fraction; PS_{act} : Active uptake intrinsic clearance at the sinusoidal membrane; $PS_{dif,eff}$: Intrinsic efflux clearance by passive diffusion through sinusoidal membrane; $PS_{dif,inf}$: Intrinsic influx clearance by passive diffusion through sinusoidal membrane; CL_{bile} : Intrinsic clearance of biliary excretion at the canalicular membrane; CL_{gall} : Intercompartment clearance from the intrahepatic bile duct to the gallbladder

Software and Parameter Estimation

The modeling/simulation and plots generation were performed using R software (Version 4.0.2) with the ordinary differential equation (ODE) solver package ‘mrgsolve’ (Version 0.8.12). Residual error was estimated using combined proportional and additive error model. The hepatobiliary clearances of RSV were estimated by simultaneously fitting to the liver and gallbladder pharmacokinetic profiles using maximum likelihood objective function with newuoa. The goodness-of-fit plots and Akaike’s Information Criterion (AIC) was used for the evaluation of fitting results.

RESULTS

Liver Input Function Assessment

The performance of the two liver input functions, AIF and DIF on the description of hepatic distribution of RSV under the control condition was compared by simulating liver concentration profiles. PS_{act} , $PS_{dif,eff}$, CL_{bile} ,

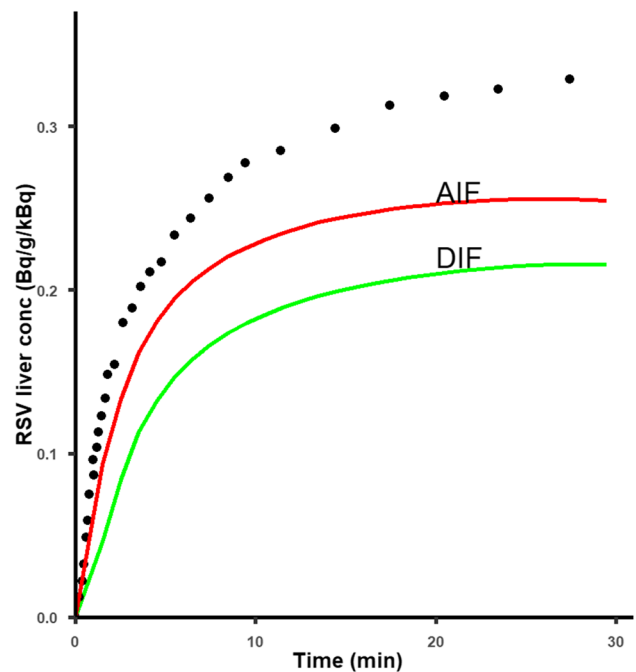
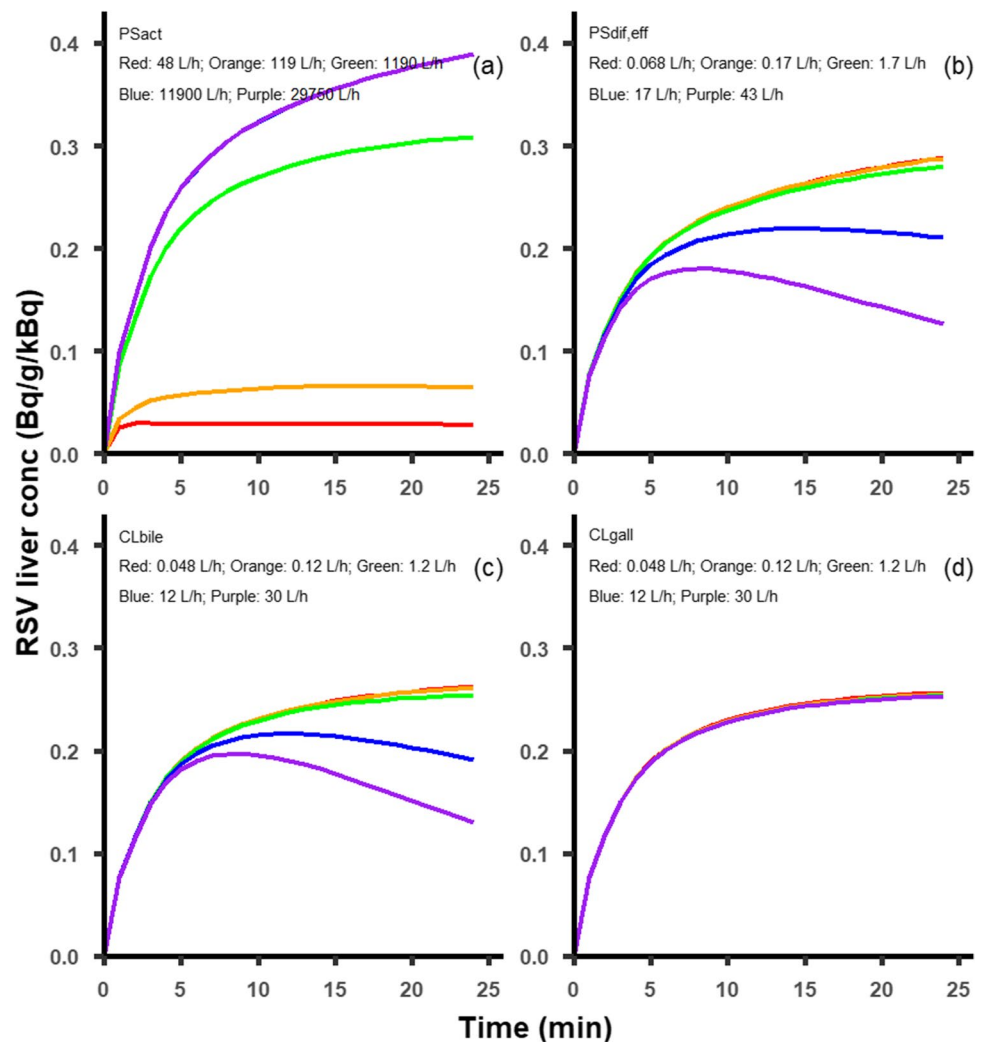


Fig. 4 Observed (solid circles) and simulated (solid line) RSV liver concentration profiles with two proposed forcing functions. Green line: Dual input function (DIF); Red line: Arterial input function (AIF)

and CL_{gall} were set as their initial values. As shown in Fig. 4, when DIF was applied as the blood supply input function in the liver model, the simulated liver concentration profiles markedly underestimated the observations throughout the sampling period. Though underestimation of the observed data still existed when AIF was used as the input function, the simulated profile was fairly close to observations at the initial distribution stage (0–4 min).

To investigate whether the underestimation problem can be addressed by altering the values of hepatobiliary clearances, the impact of PS_{act} , $PS_{dif,eff}$, CL_{bile} , and CL_{gall} on liver concentration profiles were assessed via a sensitivity analysis with a wide range of values (~0.04- to 25-fold of their initial values), while DIF was used as forcing function in the liver model. As shown in Fig. 5, the liver concentration profiles obtained from the sensitivity analysis indicated sensitivity to the values of PS_{act} , $PS_{dif,eff}$, CL_{bile} , but minimal sensitivity to CL_{gall} . A significant impact of CL_{gall} was observed on the RSV gallbladder concentration profiles (Fig. S2 in the Supplemental Materials). Interestingly, none of the tested clearances showed a noticeable impact at the initial distribution stage (0–4 min) of the liver concentration profiles, except that the simulated liver concentrations were further decreased with an extremely low PS_{act} value. Collectively, future clearance parameter optimization by fitting the liver model to clinical data was not

Fig. 5 Parameter sensitivity analysis for PS_{act} (a), $PS_{dif,eff}$ (b), CL_{bile} (c), and CL_{gall} (d) with dual input function as model input function. In each panel, all parameter values were fixed except for the test parameter. The range of test parameter values was set as ~0.04- to 25-fold of their initial values



likely to offset the underestimation of liver concentration occurred at the early distribution stage (0–4 min) for DIF. Thus, AIF was used in the following parameter estimation and simulation steps.

Fitting of the RSV Liver Model to the Hepatobiliary Profiles

The hepatobiliary clearances for RSV in the liver model were estimated via simultaneously fitting to observed liver and gallbladder profiles under the control condition after single *i.v.* administration of [^{11}C]RSV, with initial values described in Table I. All estimated parameters demonstrated good precision, except for $PS_{dif,eff}$ which showed a wider 95% CI (Table II). As shown in Fig. 1, the fitting accurately described the liver and gallbladder exposure data and corresponded to the shape of the observed profiles. As there was a 10-min delay for emergence of RSV into the gallbladder after dosing, incorporation of the intrahepatic bile duct

Table II Estimated Hepatobiliary Clearances of RSV under Control and DDI (Co-Administered with CsA) Conditions. The Results are Shown as Mean(95% Confidence Interval)

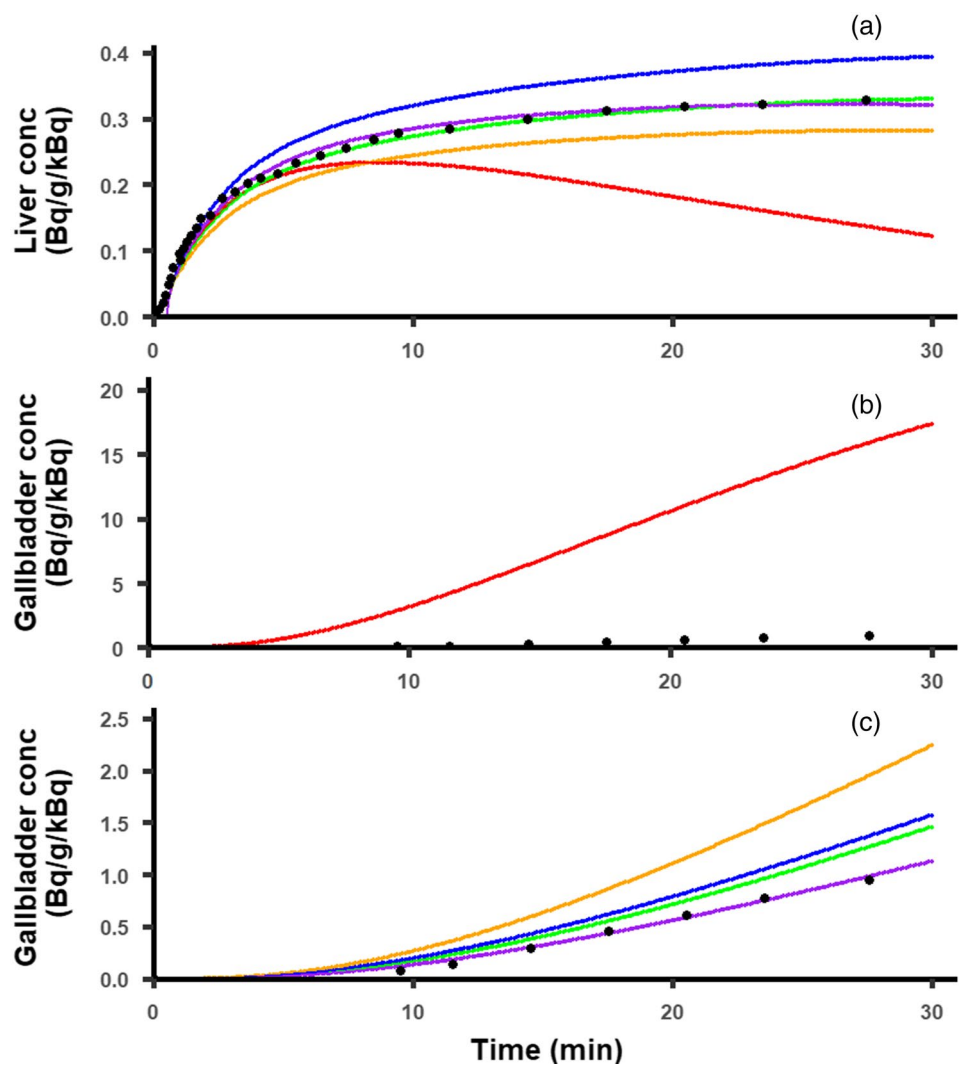
Parameters	RSV	RSV + CsA	Percent change (%)
PS_{act} (L/h)	1622 (1332–1974)	487 (466–509)	–70.0
$PS_{dif,eff}$ (L/h)	12.06 (5.64–25.74)	16.0 (14.0–18.1)	32.7
CL_{bile} (L/h)	0.90 (0.68–1.18)	0.44 (0.40–0.49)	–51.1
CL_{gall} (L/h) ^a	0.036 (0.026–0.049)	0.036 (0.026–0.049)	–

^a CL_{gall} was fixed with the optimized value under the control condition when fitting data under DDI condition, assuming that the distribution of RSV from the intrahepatic bile duct to the gallbladder was not influenced by CsA

compartment improved model fitting and led to lower AIC value (data not shown).

Fitting analysis for RSV were then performed with the hepatobiliary disposition profiles under the DDI condition. CL_{gall} was fixed with the optimized value under the

Fig. 6 Observed and simulated RSV liver (a) and gallbladder (b and c) concentration profiles with four reported liver submodels or the established model in the present study. Solid circles represent observed values. The red, blue, green, orange, and purple lines represent the simulation profiles from the models reported by Futatsugi *et al.*, Li *et al.*, Jones *et al.*, Bosgra *et al.*, or established in the present study



control condition as no evidence supported that the distribution of RSV from the intrahepatic bile duct to the gallbladder was influenced by CsA. The model fitting to the liver and gallbladder concentrations is shown in Fig. 1. Similarly, precise estimates of hepatobiliary clearances were achieved by model fitting (Table II). For RSV, hepatic uptake at the sinusoidal membrane and biliary excretion at the canalicular membrane was markedly inhibited when co-administrated with CsA, demonstrated by decreases in PS_{act} and CL_{bile} by 70.0% and 51.1%, respectively.

Evaluating the Performance in Predicting RSV Hepatobiliary Disposition of Selected PBPK Models

Evaluation of the model performance in predicting hepatobiliary disposition of RSV was performed by visual inspection of overlays of predicted and observed

tissue profiles (Fig. 6). The observed liver concentration profiles showed a pattern of rapid accumulation after dosing and the hepatic uptake seemed to reach steady state at the end of imaging stage (~25–30 min). In addition, there was a steady accumulation of RSV observed in the gallbladder via biliary excretion during the imaging period. Comparatively, the liver model reported by Jones *et al.* led to a fairly good estimation of hepatic disposition of RSV, though the extent of biliary excretion was slightly overestimated. There was a substantial deviation between simulated profiles obtained from the other three liver models and the observed hepatobiliary data: The liver concentration profiles from the models reported by Futatsugi *et al.* showed a decline phase at the later stage, while the liver model proposed by Li *et al.*/Bosgra *et al.* systematically overestimate/underestimate the liver concentration; The gallbladder concentrations were dramatically overestimated with all three liver models. The ratios of AUC or C_{max} between

simulated data and observation were not calculated as the complete liver concentration profiles (>30 min) were not available (hepatobiliary concentration were not measured beyond 30 min post dose). The selected liver submodels were also trained with the hepatobiliary data from the PET imaging study. The model fitting and estimates of hepatobiliary clearances are shown in Fig. S3 and Table S2 in the Supplemental Materials. Clearly, all the models were able to describe liver pharmacokinetics after being trained with the hepatobiliary exposure data.

DISCUSSIONS

In the last decade, PBPK models have been widely used to predict tissue exposure and assess clinical DDI for transporter substrates. As it is problematic to directly apply *in vitro* transport clearances for *in vivo* prediction in most cases, successful predictions were only achieved when empirical scaling factors were incorporated (6). Therefore, nearly all PBPK models for transporter substrates rely on systemic exposure data for initial model development/refinement and final model verification. Nevertheless, a fundamental question needs to be addressed as to whether the model trained with only systemic exposure data can reasonably simulate tissue concentration profiles. Li *et al.* introduced two sets of different values of hepatic clearance processes into one PBPK model with identical values for all other model parameters. Though plasma time course data can be well-described, substantially different concentrations in the liver were observed with the two sets of hepatic clearance values (21). The simulation work conducted by Patilea-Vrana *et al.* also demonstrated that when sinusoidal uptake was the rate-determining step in the hepatic clearance of the drug, inhibition of canalicular or sinusoidal efflux clearance was not expected to alter systemic concentration (8). In the present study, four liver submodels of PBPK models of RSV with similar model structure were selected for simulation of hepatobiliary profiles. A variety of approaches were used to estimate hepatobiliary clearances when developing these models, including scaling *in vitro* hepatobiliary clearance and fitting of *i.v.* and/or *p.o.* clinical data, a global optimization approach to obtain empirical scaling factors based on *i.v.* clinical data, and scaling *in vitro* PS_{act} based on the transporter protein expression levels (6, 9–11). Although the selected PBPK models had been verified with clinical plasma concentration data, these liver submodels predicted distinctive liver and gallbladder concentration profiles with the same liver blood input function. It is apparent that PBPK

strategies to date that exclusively use systemic exposure data is not completely reliable in predicting hepatic disposition processes or liver concentration. If not addressed, inaccurate hepatobiliary disposition predictions may influence model building to describe enterohepatic circulation and metabolite pharmacokinetics. More importantly, uncertainty in predicting hepatic disposition may be carried into further PBPK model application (e.g., DDI prediction and liver concentration in special population).

To address the problem, tissue exposure data measured by noninvasive nuclear imaging methods are vital for the purpose of examining and verifying liver models and estimating transporter-mediated clearances. The imaging technology is able to provide quantitative information in the liver and gallbladder to support estimation of hepatobiliary clearances. In addition, using hepatic blood supply as the model input, hepatobiliary clearances can be estimated in such a liver submodel which purely describes the hepatobiliary disposition process, minimizing the confounding effects on systemic exposure such as oral absorption (including enterohepatic circulation), distribution occurring in other tissues, and extra-hepatic elimination. A similar approach has been used to successfully estimate kinetic distribution parameters in tissues for CsA by fitting tissue concentration-time data of each organ with arterial plasma concentration-time profiles as model input function (20). Admittedly, extensive hepatic metabolism needs to be avoided or better monitored by surrogate measurement as imaging technologies cannot differentiate between parent drug and metabolites.

There have been several reports on estimation of hepatic clearances of transporter substrates based on PET imaging data, in which hepatic clearances were evaluated by the integration plot method or empirical compartment analysis (treating the liver as single compartment). The estimated values were not to be directly applied to PBPK models (1, 22–24). To bridge such a disconnect, the commonly applied liver submodel in PBPK models of RSV was used to determine hepatobiliary clearances of RSV based on the hepatic disposition data obtained from PET imaging in this study (1). Some modifications were made in the liver model based on the properties of the data: (i) Using AIF as the driving force for hepatic blood input; (ii) Adding two compartments to reflect the distribution of RSV in the intrahepatic bile duct and gallbladder. Both AIF and DIF (using concentrations in peripheral venous or mathematical methods to represent the concentrations in portal vein) have been used as hepatic blood input function (1, 22–24). As the liver receives blood from the hepatic artery (~20%) and the portal vein (~80%),

DIF seems to be a more accurate source of drug to the liver model as it mimics physiological conditions better. However, a previous PET imaging study to describe the hepatic disposition of [^{11}C]erlotinib showed that there were no statistically significant differences in the model performance when AIF or DIF (using a mathematical method to represent the exposure level in portal vein) was implemented based on AIC values. In the present study, the model performance of predicting liver concentration with AIF and DIF (using peripheral venous concentrations to represent the concentrations in portal vein) was compared. The results demonstrated that DIF led to a substantial underestimation of liver concentration at the initial stage after *i.v.* dosing which cannot be offset by optimization of model parameter values, indicating that peripheral venous concentrations might not be a good representative of the concentrations in portal vein. Though [^{11}C]RSV in the intrahepatic bile ducts was not directly visible in the PET scans, it had been suggested that adding this compartment may provide a richer kinetic picture and account for the total liver radioactivity (23). In this study, the gallbladder concentrations were not measurable at the initial imaging period (within ~10 min after dosing). Visual inspection of the model fits and comparison with AIC values indicated that incorporation of the intrahepatic bile duct compartment improved model fits (data not shown).

In the present study, application of hepatobiliary exposure data significantly improves the predictive performance of hepatobiliary disposition of rosuvastatin. As the liver submodels developed in the present study and the models reported by Jones *et al.* and Futatsugi *et al.* shared the same model structure, the parameter values estimated in this study and reported in the two studies were compared to elucidate the impact of hepatobiliary data on model parameter estimation (6, 10). The value of PS_{act} were consistent among the three models, ranging from 1190 L/h to 1622 L/h, indicating that fitting of either systemic or tissue (hepatobiliary) data is adequate to estimate this parameter in the current model. This is because the systemic exposure is merely determined by sinusoidal uptake for rosuvastatin so that PS_{act} is sensitive to the change in systemic concentration. On the contrary, a marked discrepancy was observed in the estimated values from the three models for $\text{PS}_{\text{dif,eff}}$ and CL_{bile} which fail to show a significant impact on systemic exposure, indicating the necessity of using hepatobiliary data to accurately predict the intrinsic hepatobiliary clearances. When the four liver submodels from of RSV with similar model structure were trained with hepatobiliary data, all models were able to accurately predict liver pharmacokinetics. A permeability-limited

distribution between intracellular liver sub-compartments was assumed in the model reported by Li *et al.* (11). However, this assumption seemed not to lead to additionally improvement in model predictive performance when comparing the model developed in the present study. In addition, whether the liver compartment was subdivided into four or five units of extracellular and intracellular compartments show a limited influence on the model predictive performance. Collectively, it is important to utilize hepatobiliary data for accurate prediction of the hepatobiliary clearances, especially when these hepatobiliary clearances are not the rate-determining step in the hepatic clearance of the drug but still show a significant impact on hepatic disposition of the drug.

Based on the hepatobiliary clearances of RSV estimated under both control and DDI conditions, CsA markedly decreased PS_{act} and CL_{bile} , showing as 70.0% and 51.1% reduction, respectively. CsA is known as an inhibitor of OATP1B1, NTCP, BCRP, P-gp, and MRP2, with reported IC_{50} values of 0.21 μM , 0.37 μM , 1.5 μM , 3.2 μM , and 5.6 μM , respectively (1). As the liver-to-blood partition coefficient for unbound drug for CsA is 1.80, the unbound hepatic concentration of CsA was expected to be much higher than its blood concentration (CsA unbound blood concentrations during imaging was ~0.17 μM) (1, 25, 26). Therefore, it was not surprising that both sinusoidal uptake and canalicular efflux of RSV were blocked by CsA. In the original PET imaging study of RSV, the change in sinusoidal uptake clearance and biliary efflux clearance of RSV in the presence of CsA was calculated as -25.29% (ranging from 6% to -48%) and -51.6% (ranging from -30% to -67%) based on data from all subjects (1). A much larger inhibitory effect on sinusoidal uptake clearance (decreases by 70.0%) was estimated in this study, which might be due to the different modeling strategies applied (empirical compartment analysis vs. mechanistic modeling analysis). However, given that CsA showed low IC_{50} values for OATPs and its high unbound hepatic exposure level, the prediction of *in vivo* inhibitory effects of CsA in the present study could represent the true DDI magnitude observed in the PET imaging study of RSV.

One limitation of the modeling reported here is that the complete pharmacokinetic dataset (e.g., blood, liver, and gallbladder) was available only from single subject. More hepatic disposition data are required to confirm and refine model prediction of hepatobiliary profiles in future studies. However, given that similar liver and gallbladder concentration profiles were observed between the selected subject and other participants in the study ($n=5$) and there

was relatively low variability in blood concentration profiles (coefficient of variation (CV) < 30% for both AUC and C_{\max} , except that CV was 41% for C_{\max} under the DDI condition), the hepatobiliary disposition of [^{11}C]RSV in the selected subject appeared to be representative of the entire participant population. Another limitation is that since imaging cannot directly measure RSV metabolites in the liver, the assumption that no hepatic metabolism of RSV occurred during the imaging period was based on the quantification of RSV metabolites in the plasma (1).

CONCLUSIONS

The present study highlights the inadequate predictive performance of hepatobiliary disposition of RSV when PBPK models were trained with only systemic exposure data by comparing the predicted hepatobiliary profiles with clinical observations. Accordingly, a new approach was proposed to estimate hepatobiliary clearances via fitting a mechanistic liver model used in PBPK modeling to the liver and the gallbladder pharmacokinetic profiles obtained by PET imaging. In the future, the optimized hepatobiliary clearances data could be used to refine PBPK models of RSV. Furthermore, the approach may be extended to other transporter substrates, for which tissue exposure data are available.

Acknowledgements and Disclosures The authors thank Dr. Kyle Baron at Metrum Research Group for providing the technical support for R package ‘mrg-solve’. The authors thank Dr. Elimika Fletcher from the US FDA, Office of Clinical Pharmacology, for the comments and suggestions in the revision of this manuscript. The views expressed in this paper are those of the authors and do not necessarily represent those of the FDA. The authors declare that they have no conflict of interest.

Author Contributions *Participated in research design:* Wang, Zhu, Tran, Seo and Pan.

Performed data analysis: Wang, Zhu, and Pan.

Wrote or contributed to the writing of the manuscript: Wang, Tran, Seo and Pan.

Funding This work was supported by the FDA Summer Intern Program.

REFERENCES

1. Billington S, Shoner S, Lee S, Clark-Snustad K, Pennington M, Lewis D, Muzi M, Rene S, Lee J, Nguyen TB, Kumar V, Ishida K, Chen L, Chu X, Lai Y, Salphati L, Hop C, Xiao G, Liao M, Unadkat JD. Positron emission tomography imaging of [(11)C]Rosuvastatin hepatic concentrations and hepatobiliary Transport in humans in the absence and presence of Cyclosporin a. *Clin Pharmacol Ther.* 2019;106(5):1056–66.
2. Guo Y, Chu X, Parrott NJ, KLR B, Hsu V, Nagar S, Matsson P, Sharma P, Snoeys J, Sugiyama Y, Tatosian D, Unadkat JD, Huang SM, Galetin A, International Transporter C. Advancing predictions of tissue and intracellular drug concentrations using in vitro, imaging and physiologically based pharmacokinetic modeling approaches. *Clin Pharmacol Ther.* 2018;104(5):865–89.
3. Cho SK, Kim CO, Park ES, Chung JY. Verapamil decreases the glucose-lowering effect of metformin in healthy volunteers. *Br J Clin Pharmacol.* 2014;78(6):1426–32.
4. Hibma JE, Zur AA, Castro RA, Wittwer MB, Keizer RJ, Yee SW, Goswami S, Stocker SL, Zhang X, Huang Y, Brett CM, Savic RM, Giacomini KM. The effect of famotidine, a MATE1-selective inhibitor, on the pharmacokinetics and pharmacodynamics of metformin. *Clin Pharmacokinet.* 2016;55(6):711–21.
5. Zamek-Gliszczynski MJ, Lee CA, Poirier A, Bentz J, Chu X, Ellens H, Ishikawa T, Jamei M, Kalvass JC, Nagar S, Pang KS, Korzekwa K, Swaan PW, Taub ME, Zhao P, Galetin A, International Transporter C. ITC recommendations for transporter kinetic parameter estimation and translational modeling of transport-mediated PK and DDIs in humans. *Clin Pharmacol Ther.* 2013;94(1):64–79.
6. Jones HM, Barton HA, Lai Y, Bi YA, Kimoto E, Kempshall S, Tate SC, El-Kattan A, Houston JB, Galetin A, Fenner KS. Mechanistic pharmacokinetic modeling for the prediction of transporter-mediated disposition in humans from sandwich culture human hepatocyte data. *Drug Metab Dispos.* 2012;40(5):1007–17.
7. Watanabe T, Kusuhara H, Maeda K, Shitara Y, Sugiyama Y. Physiologically based pharmacokinetic modeling to predict transporter-mediated clearance and distribution of pravastatin in humans. *J Pharmacol Exp Ther.* 2009;328(2):652–62.
8. Patilea-Vrana G, Unadkat JD. Transport vs. Metabolism: what determines the pharmacokinetics and pharmacodynamics of drugs? Insights from the extended clearance model. *Clin Pharmacol Ther.* 2016;100(5):413–8.
9. Bosgra S, van de Steeg E, Vlaming ML, Verhoeckx KC, Huisman MT, Verwei M, Wortelboer HM. Predicting carrier-mediated hepatic disposition of rosuvastatin in man by scaling from individual transfected cell-lines in vitro using absolute transporter protein quantification and PBPK modeling. *Eur J Pharm Sci.* 2014;65:156–66.
10. Futatsugi A, Toshimoto K, Yoshikado T, Sugiyama Y, Kato Y. Evaluation of alteration in hepatic and intestinal BCRP function in vivo from ABCG2 c.421C>a polymorphism based on PBPK analysis of Rosuvastatin. *Drug Metab Dispos.* 2018;46(5):749–57.
11. Li R, Barton HA, Yates PD, Ghosh A, Wolford AC, Riccardi KA, Maurer TS. A "middle-out" approach to human pharmacokinetic predictions for OATP substrates using physiologically-based pharmacokinetic modeling. *J Pharmacokinet Pharmacodyn.* 2014;41(3):197–209.
12. Kitamura S, Maeda K, Wang Y, Sugiyama Y. Involvement of multiple transporters in the hepatobiliary transport of rosuvastatin. *Drug Metab Dispos.* 2008;36(10):2014–23.

13. Ho RH, Tirona RG, Leake BF, Glaeser H, Lee W, Lemke CJ, Wang Y, Kim RB. Drug and bile acid transporters in rosuvastatin hepatic uptake: function, expression, and pharmacogenetics. *Gastroenterology*. 2006;130(6):1793–806.
14. Ieiri I, Higuchi S, Sugiyama Y. Genetic polymorphisms of uptake (OATP1B1, 1B3) and efflux (MRP2, BCRP) transporters: implications for inter-individual differences in the pharmacokinetics and pharmacodynamics of statins and other clinically relevant drugs. *Expert Opin Drug Metab Toxicol*. 2009;5(7):703–29.
15. Pfeifer ND, Yang K, Brouwer KL. Hepatic basolateral efflux contributes significantly to rosuvastatin disposition I: characterization of basolateral versus biliary clearance using a novel protocol in sandwich-cultured hepatocytes. *J Pharmacol Exp Ther*. 2013;347(3):727–36.
16. Schenk WG Jr, Mc DJ, Mc DK, Drapanas T. Direct measurement of hepatic blood flow in surgical patients: with related observations on hepatic flow dynamics in experimental animals. *Ann Surg*. 1962;156:463–71.
17. Mattsson S, Johansson L, Leide Svegborn S, Liniecki J, Nosske D, Riklund KA, Stabin M, Taylor D, Bolch W, Carlsson S, Eckerman K, Giussani A, Soderberg L, Valind S, ICRP. Radiation dose to patients from radiopharmaceuticals: a compendium of current information related to frequently used substances. *Ann ICRP*. 2015;44(2 Suppl):7–321.
18. Orntoft NW, Munk OL, Frisch K, Ott P, Keiding S, Sorensen M. Hepatobiliary transport kinetics of the conjugated bile acid tracer (11)C-CSar quantified in healthy humans and patients by positron emission tomography. *J Hepatol*. 2017;67(2):321–7.
19. Davies B, Morris T. Physiological parameters in laboratory animals and humans. *Pharm Res*. 1993;10(7):1093–5.
20. Kawai R, Mathew D, Tanaka C, Rowland M. Physiologically based pharmacokinetics of cyclosporine a: extension to tissue distribution kinetics in rats and scale-up to human. *J Pharmacol Exp Ther*. 1998;287(2):457–68.
21. Li R, Maurer TS, Sweeney K, Barton HA. Does the systemic plasma profile inform the liver profile? Analysis using a physiologically based pharmacokinetic model and individual compounds. *AAPS J*. 2016;18(3):746–56.
22. Kaneko K, Tanaka M, Ishii A, Katayama Y, Nakaoka T, Irie S, Kawahata H, Yamanaga T, Wada Y, Miyake T, Toshimoto K, Maeda K, Cui Y, Enomoto M, Kawamura E, Kawada N, Kawabe J, Shiomi S, Kusuhara H, et al. A clinical quantitative evaluation of hepatobiliary Transport of [(11)C]Dehydrop-ravastatin in humans using positron emission tomography. *Drug Metab Dispos*. 2018;46(5):719–28.
23. Hernandez Lozano I, Karch R, Bauer M, Blaickner M, Matsuda A, Wulkersdorfer B, Hacker M, Zeitlinger M, Langer O. Towards improved pharmacokinetic models for the analysis of transporter-mediated hepatic disposition of drug molecules with positron emission tomography. *AAPS J*. 2019;21(4):61.
24. Bauer M, Matsuda A, Wulkersdorfer B, Philippe C, Traxl A, Ozvegy-Laczka C, Stanek J, Nics L, Klebermass EM, Poschner S, Jager W, Patik I, Bakos E, Szakacs G, Wadsak W, Hacker M, Zeitlinger M, Langer O. Influence of OATPs on hepatic disposition of Erlotinib measured with positron emission tomography. *Clin Pharmacol Ther*. 2018;104(1):139–47.
25. Riede J, Poller B, Huwyler J, Camenisch G. Assessing the risk of drug-induced cholestasis using unbound intrahepatic concentrations. *Drug Metab Dispos*. 2017;45(5):523–31.
26. Yoshikado T, Yoshida K, Kotani N, Nakada T, Asaumi R, Toshimoto K, Maeda K, Kusuhara H, Sugiyama Y. Quantitative analyses of hepatic OATP-mediated interactions between statins and inhibitors using PBPK modeling with a parameter optimization method. *Clin Pharmacol Ther*. 2016;100(5):513–23.
27. Caroli-Bosc FX, Pugliese P, Peten EP, Demarquay JF, Montet JC, Hastier P, Staccini P, Delmont JP. Gallbladder volume in adults and its relationship to age, sex, body mass index, body surface area and gallstones. An epidemiologic study in a non-selected population in France. *Digestion*. 1999;60(4):344–8.

Publisher's Note Springer Nature remains neutral with regard to jurisdictional claims in published maps and institutional affiliations.